NASA TECHNICAL NOTE

NASA TN D-6622

NASA TN D-6622

THREE-DIMENSIONAL POTENTIAL AND CURRENT DISTRIBUTIONS IN A HALL GENERATOR WITH ASSUMED VELOCITY PROFILES

by N. Stankiewicz and R. W. Palmer

Lewis Research Center
Cleveland, Ohio 44135

NATIONAL AERONAUTICS AND SPACE ADMINISTRATION • WASHINGTON, D. C. • JANUARY 1972

1. Report No.	2. Government Accession No.	3. Recipient's Catalog No.
NASA TN D-6622		

4. Title and Subtitle	5. Report Date
THREE-DIMENSIONAL POTENTIAL AND CURRENT DISTRIBUTIONS IN A HALL GENERATOR WITH ASSUMED VELOCITY PROFILES	January 1972
	6. Performing Organization Code

7. Author(s)	8. Performing Organization Report No.
N. Stankiewicz and R. W. Palmer	E-6551
	10. Work Unit No. 112-02

9. Performing Organization Name and Address	11. Contract or Grant No.
Lewis Research Center National Aeronautics and Space Administration Cleveland, Ohio 44135	

12. Sponsoring Agency Name and Address	13. Type of Report and Period Covered
National Aeronautics and Space Administration Washington, D. C. 20546	Technical Note
	14. Sponsoring Agency Code

15. Supplementary Notes

16. Abstract

Three-dimensional potential and current distributions in a Faraday segmented MHD generator operating in the Hall mode are computed. Constant conductivity and a Hall parameter of 1.0 is assumed. The electric fields and currents are assumed to be coperiodic with the electrode structure. The flow is assumed to be fully developed and a family of power-law velocity profiles, ranging from parabolic to turbulent, is used to show the effect of the fullness of the velocity profile. Calculation of the square of the current density shows that nonequilibrium heating is not likely to occur along the boundaries. This seems to discount the idea that the generator insulating walls are regions of high conductivity and are therefore responsible for "boundary-layer shorting", unless the shorting is a surface phenomenon on the insulating material.

17. Key Words (Suggested by Author(s))	18. Distribution Statement
	Unclassified - unlimited

19. Security Classif. (of this report)	20. Security Classif. (of this page)	21. No. of Pages	22. Price*
Unclassified	Unclassified	33	$3.00

* For sale by the National Technical Information Service, Springfield, Virginia 22151

THREE-DIMENSIONAL POTENTIAL AND CURRENT DISTRIBUTIONS IN A HALL GENERATOR WITH ASSUMED VELOCITY PROFILES

by N. Stankiewicz and R. W. Palmer

Lewis Research Center

SUMMARY

Three-dimensional potential and current distributions in a Faraday segmented magnetohydrodynamics (MHD) generator operating in the Hall mode are computed. Constant conductivity and a Hall parameter of 1.0 is assumed. The electric fields and currents are assumed to be coperiodic with the electrode structure. The flow is assumed to be fully developed and a family of power-law velocity profiles, ranging from parabolic to turbulent, is used to show the effect of the fullness of the velocity profile. Calculation of the square of the current density shows that nonequilibrium heating is not likely to occur along the boundaries. This seems to discount the idea that the generator insulating walls are regions of high conductivity and therefore responsible for "boundary-layer shorting", unless the shorting is a surface phenomenon on the insulating material.

INTRODUCTION

Two-dimensional potential and current distributions within a magnetohydrodynamic (MHD) generator channel have been investigated in many studies (see, e.g., refs. 1 to 4). These two-dimensional results are adequate if the velocity profile is constant in the magnetic-field direction. Unfortunately, the viscous effects of the side walls cannot be ignored in a real MHD channel because of its finite width.

It is suspected that the shorting noticed in real generators is caused by the velocity profiles in the channel. Near the insulator sidewalls, the smaller stream velocity causes a reduction in the Faraday component of the current (see fig. 1). This, in turn, reduces the $\vec{j} \times \vec{B}$ force against which the stream does work. A Hall potential is induced in the downstream electrodes as the result of this work. For a given Hall current, the Hall potential will therefore be less than the expected value without insulator sidewalls.

Conversely, for a given Hall potential, the Hall current will be higher as a result of the sidewalls, giving the appearance of a short circuit.

Because of the importance of the shorting problem in the operation of an actual generator, it is necessary that the effect of the sidewalls be studied. This necessitates a three-dimensional analysis.

The problem studied in this report is a constant conductivity, fully developed flow problem in which the velocity profile varies only transverse to the flow. It is shown in reference 5 that a three-dimensional analysis is not necessary if one is only interested in the overall duct characteristics (load lines); that is, by averaging over the third dimension (parallel to the magnetic field) the problem can be reduced to a two-dimensional problem. This method, however, does not determine the local potential and current distributions. It is the local current distribution that affects the local conductivity and efficiency.

The purpose of this study is to solve the three-dimensional potential problem when the velocity profile varies across the duct. However, rather than solve the coupled momentum equation for the actual velocity profile, a power-law variation is assumed. That is, the velocity varies as a power of the distance from a wall. This is valid because the interaction parameters between the plasma equations and the fluid equations are small. The essential features of a three-dimensional problem are retained with this assumption.

The exponent in the velocity function is a parameter in this study. A value of 1.0 for the exponent yields a parabolic velocity profile; and a value of 1/7 is a good approximation to turbulent flow across a flat plate. For turbulent flow in a channel with a square cross section the power seems closer to 1/6 (ref. 6). Varying the velocity profile changes the effective size of the region in which shorting is expected.

SYMBOLS

A(K, L, M)	computational definition of normalized potential function used in finite difference forms of differential equations
a	dimension of duct in y direction
B	magnetic field
b	dimension of duct in x direction
C	number of points into which a unit line is divided for computational use
D	damping factor
E	electric field
e	electron charge

h	dimension of duct in z direction
I	total current
J	normalized total current density
j	current density
K	integer point location in normalized x direction
K_H	Hall load factor
K_o	constant (eq. (4))
L	integer point location in normalized y direction
M	integer point location in normalized z direction
M_e	electron mass
m	exponential parameter in velocity distribution
t	time
U	normalized velocity
u	velocity
V	present value of normalized potential function
(x, y, z)	coordinates, $(x \mid\mid \vec{B};\ y \mid\mid \vec{u};\ z \mid\mid \vec{B} \times \vec{u})$

Greek Symbols

β	Hall parameter
γ	ratio h/a
μ	ratio h/b
ν_{ei}	electron-ion collision frequency
(ξ, η, ζ)	normalized coordinates, $(\xi \mid\mid \vec{B};\ \eta \mid\mid \vec{u};\ \zeta \mid\mid \vec{B} \times \vec{u})$
σ	conductivity
φ	potential function
ψ	normalized potential function

Math Symbol

$\langle\ \rangle$	average value of

Subscripts:

i	ion
e	electron
F	Faraday
H	Hall
(x,y,z)	vector component

Superscripts:

$\rightarrow$	vector
$\hat{}$	unit vector
i	iteration number

ANALYSIS

Derivation of Equations

The fundamental equations used in the analysis of an MHD generator are the continuity of current

$$\operatorname{div} \vec{j} = 0 \tag{1}$$

and the Ohm's law relating current and electric field through a vector conductivity. Equation (1) can be written in terms of a scalar conductivity as

$$\vec{j} = \sigma (\vec{E} + \vec{u} \times \vec{B}) - \frac{e}{M_e \nu_{ei}} \vec{j} \times \vec{B} \tag{2}$$

In addition, the basic equation of electrodynamics $\operatorname{curl} \vec{E} = 0$ allows the defining of $\vec{E}$ with a scalar potential φ,

$$\vec{E} = -\operatorname{grad} \varphi \tag{3}$$

The coordinate system and field orientation are shown in figure 1. The flow is perpendicular to the magnetic field.

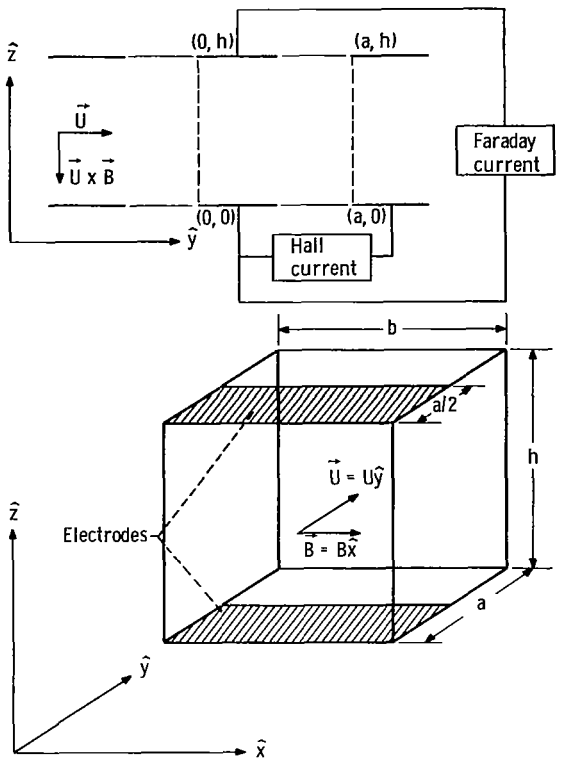

Figure 1. - Coordinate system and channel orientation.

The velocity vector $\vec{u}$ is chosen in the positive y direction and a constant magnetic field $\vec{B}$ in the positive x direction. The pressure, temperature, conductivity, and channel cross section are held constant. End effects of the channel are ignored.

A power-law velocity profile of the form given in equation (4) is assumed. The profile is constant in the y direction.

$$u = K_o[x(b - x)]^{1/m}[z(h - z)]^{1/m} \tag{4}$$

Equation (4) yields a parabolic profile when $m = 1$ and a turbulent profile when $m = 7$.

Equation (4) can be normalized to the average velocity $\langle u \rangle$ by means of this definition:

$$\langle u \rangle = \frac{K_o}{bh}\int_{x=0}^{b}\int_{z=0}^{h} dx\, dz\,[x(b - x)]^{1/m}[z(h - z)]^{1/m} \tag{5}$$

Eliminating K_o with equation (5), equation (4) becomes

$$u = \langle u \rangle bh \frac{[x(b - x)]^{1/m}[z(h - z)]^{1/m}}{\int_0^b \int_0^h [x(b - x)]^{1/m}[z(h - z)]^{1/m}\, dx\, dz} \tag{6}$$

Taking the dot product, and cross product of equation (2) with $\vec{B}$ and solving for $\vec{j} \cdot \vec{B}$ and $\vec{j} \times \vec{B}$ one can solve the identity $\vec{B} \times (\vec{j} \times \vec{B}) = \vec{j} B^2 - \vec{B}(\vec{j} \cdot \vec{B})$ to get

$$\vec{j} = \frac{\sigma}{1 + \beta^2}\left[\vec{E} + \vec{u} \times \vec{B} + \beta B\vec{u} + \frac{\beta}{B}\vec{B} \times \vec{E} + \frac{\beta^2}{B^2}\vec{B}(\vec{E} \cdot \vec{B})\right] \tag{7}$$

where the condition $\vec{U} \cdot \vec{B} = 0$ is used, and $\beta = eB/M_e\nu_{ei}$ is the Hall parameter.

Using equation (3), equation (7) in component form becomes

$$j_x = -\sigma \frac{\partial \varphi}{\partial x} \tag{8}$$

$$j_y = \frac{\sigma}{1 + \beta^2}\left(-\frac{\partial \varphi}{\partial y} + \beta \frac{\partial \varphi}{\partial z} + uB\beta\right) \tag{9}$$

$$j_z = \frac{\sigma}{1 + \beta^2}\left(-\beta \frac{\partial \varphi}{\partial y} - \frac{\partial \varphi}{\partial z} - uB\right) \tag{10}$$

Using equations (8) to (10) and remembering that $u = u(x, z)$, equation (1) becomes

$$(1 + \beta^2)\frac{\partial^2 \varphi}{\partial x^2} + \frac{\partial^2 \varphi}{\partial y^2} + \frac{\partial^2 \varphi}{\partial z^2} = -B \frac{\partial u}{\partial z} \tag{11}$$

The solution of equation (11) with suitable boundary conditions will give the potential distribution within the MHD channel.

The Hall current I_H is defined as the total current that passes from one unit cell $a \times b \times h$ to the next unit cell. The surface integral of the current density normal to the plane $y = 3a/4$ (the midplane of the electrode insulators) is taken as the Hall current.

Hence,

$$I_H = \int_0^b dx \int_0^h dz\, j_y\left(x, \frac{3a}{4}, z\right) \tag{12}$$

Except for the numerical difficulties of integrating over the rapidly changing fields near the electrodes, each plane y = constant along the electrode insulators $(a/2) < y < a$ should give the same value as equation (12). This can be shown by integrating div $\vec{j}$ over a volume element $bh\,\Delta y$ (i.e., two adjacent planes).

The Faraday current I_F is defined as the total current emitted by one of the electrodes in a unit cell. This current must be equal to the current flowing in the external Faraday circuit of the generator. In order to avoid the numerical difficulties when integrating near the electrodes, the Faraday current is calculated at the midplane of the cell $z = h/2$.

$$I_F = \int_0^a dy \int_0^b dx\, j_z\left(x, y, \frac{h}{2}\right) \tag{13}$$

Again it can be shown, by integrating div $\vec{j}$ over adjacent planes z = constant, that equation (13) should be equal for each plane.

Boundary Conditions

In the Hall mode of generator operation, opposite pairs of electrodes (opposite in the Faraday sense) are shorted, and the potential is allowed to build up in the Hall direction. Referring to figure 1, the Faraday electrodes are located at $z = 0$ and $z = h$ with $y = a/2$. (The lines located at $z = 0$ and $z = h$ and at $y = a$ are the leading edges of the next pair of electrodes.)

The potential of the first pair of electrodes is taken to be zero, and this provides a Dirichlet condition for the problem; that is,

$$\varphi = 0 \quad \text{at} \quad z = 0, h \tag{14}$$

$$0 \le y \le \frac{a}{2}$$

The current density normal to the sidewall insulators located at $x = o$ and $x = b$ mush vanish. Using equation (8) yields the Neumann condition:

$$\frac{\partial \varphi}{\partial x} = 0 \qquad x = o, b \tag{15}$$

Likewise the normal current j_z to the insulator spacing between electrodes must also vanish. Using equation (10) and noting from equation (6) that the velocity vanishes on the boundary yields the condition

$$\beta \frac{\partial \varphi}{\partial y} + \frac{\partial \varphi}{\partial z} = 0; \; z = o, h; \; \frac{a}{2} < y < a \tag{16}$$

The final boundary condition relates the cell entrance region ($y = 0$) to the cell exit region ($y = a$), shown in figure 1, by a periodic condition, namely,

$$\varphi(x, a, z) = \varphi(x, o, z) + \varphi_H \tag{17}$$

where φ_H is the Hall potential.

Transforming to Nondimensional Variables

The Hall potential has ideal maximum that can be found from equation (9) when $u = \langle u \rangle$, $j_y = 0$ (open circuit), and $\partial \varphi / \partial z = 0$ (no local Faraday field). In this case, equation (9) becomes

$$\frac{\partial \varphi}{\partial y} = \langle u \rangle B \beta \tag{18}$$

Integrating over one cell length gives the ideal maximum:

$$\left(\varphi_H\right)_{max} = \langle u \rangle B \beta a \tag{19}$$

The coordinates (x, y, z) are transformed with respect to the channel dimensions (b, a, h) (see fig. 1). Hence,

$$x = b\xi \tag{20}$$

$$y = a\eta \tag{21}$$

$$z = h\zeta \tag{22}$$

The ratio of channel height to width is given the symbol

$$\mu = \frac{h}{b} \tag{23}$$

And the ratio of channel height to length is given the symbol

$$\gamma = \frac{h}{a} \tag{24}$$

The potential function φ is nondimensionalized by the substitution

$$\varphi = \langle u \rangle Bh\psi \tag{25}$$

The velocity function u is nondimensionalized with respect to $\langle u \rangle$; that is,

$$u = \langle u \rangle U \tag{26}$$

With these definitions and equation (6), the normalized function U becomes

$$U = \frac{[\xi(1 - \xi)]^{1/m}[\zeta(1 - \zeta)]^{1/m}}{\int_0^1 \int_0^1 [\xi(1 - \xi)]^{1/m}[\zeta(1 - \zeta)]^{1/m} \, d\xi \, d\zeta} \tag{27}$$

Figure 2 is a plot of equation (25) at $\zeta = 1/2$. Equation (11) becomes

$$\mu^2(1 + \beta^2) \frac{\partial^2\psi}{\partial\xi^2} + \gamma^2 \frac{\partial^2\psi}{\partial\eta^2} + \frac{\partial^2\psi}{\partial\zeta^2} = -\frac{\partial U}{\partial\zeta} \tag{28}$$

The boundary conditions (eqs. (14), (15), (16), and (17)) become

$$\psi = 0; \ \zeta = 0,1; \ 0 \le \eta \le \frac{1}{2} \tag{29}$$

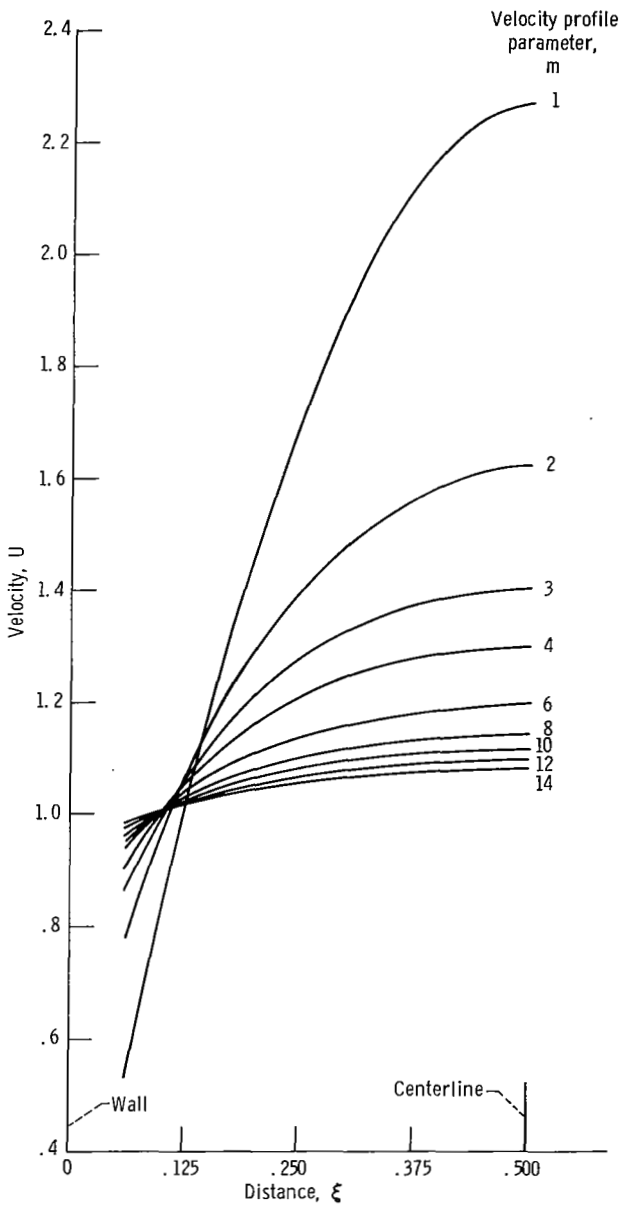

Figure 2. - Normalized velocity profile across center of cell. Normalized coordinate, ζ, 1/2.

$$\frac{\partial \psi}{\partial \xi} = 0; \ \xi = 0,1 \tag{30}$$

$$\beta\gamma \frac{\partial \psi}{\partial \eta} + \frac{\partial \psi}{\partial \zeta} = 0; \ \zeta = 0,1; \ \frac{1}{2} < \eta < 1 \tag{31}$$

$$\psi(\xi,1,\zeta) = \psi(\xi,0,\zeta) + \psi_H \tag{32}$$

The maximum value of ψ_H is then

$$\left(\psi_H\right)_{max} = \frac{\beta}{\gamma} \tag{33}$$

where equations (19), (24), and (25) were used.

The Hall current I_H is nondimensionalized by letting

$$I_H = \sigma \langle u \rangle BbhJ_H \tag{34}$$

then

$$J_H = +\frac{1}{1+\beta^2} \int_0^1 \int_0^1 \left(-\gamma \frac{\partial \psi}{\partial \eta} + \beta \frac{\partial \psi}{\partial \zeta} + \beta U\right) d\xi \, d\zeta \tag{35}$$

where the integral is computed at $\eta = 3/4$.

Similarly, the Faraday current I_F is nondimensionalized by defining

$$I_F = \sigma \langle u \rangle BabJ_F \tag{36}$$

then

$$J_F = -\frac{1}{1+\beta^2} \int_0^1 \int_0^1 \left(\beta\gamma \frac{\partial \psi}{\partial \eta} \eta + \frac{\partial \psi}{\partial \zeta} + U\right) d\xi \, d\eta \tag{37}$$

The integral, equation (35) is carried out over the plane $\zeta = 1/2$.

Finite Difference Form of the Equations

Each of the normalized coordinates $(\xi, \eta\ \zeta)$ spanning the region in figure 1 are divided into C - 1 equal line segments.

$$\xi = \frac{K - 1}{C - 1} \tag{38}$$

$$\eta = \frac{L - 1}{C - 1} \tag{39}$$

$$\zeta = \frac{M - 1}{C - 1} \tag{40}$$

where (K, L, M) are integers ranging from 1 to C. The space is therefore subdivided into a mesh having C^3 points and the index of each point is given by (K, L, M).

The potential $\psi(\xi, \eta, \zeta)$ is replaced by an array $A(K, L, M)$; and the increments $\Delta\xi$, $\Delta\eta$, $\Delta\zeta$ are equal to $1/(C - 1)$.

Three point Lagrangian differentiation formulas (see p. 914, ref. 7) are used to approximate the partial derivatives.

$$\frac{\partial^2\psi}{\partial\xi^2} \cong \frac{A(K + 1, L, M) + A(K - 1, L, M) - 2A(K, L, M)}{(\Delta\xi)^2} \tag{41}$$

$$\frac{\partial^2\psi}{\partial\eta^2} \cong \frac{A(K, L + 1, M) + A(K, L - 1, M) - 2A(K, L, M)}{(\Delta\eta)^2} \tag{42}$$

$$\frac{\partial^2\psi}{\partial\zeta^2} \cong \frac{A(K, L, M + 1) + A(K, L, M - 1) - 2A(K, L, M)}{(\Delta\zeta)^2} \tag{43}$$

Substituting these approximations into the differential equation (eq. (28)), and solving for $A(K, L, M)$, the potential at the point (K, L, M) can be written in terms of its neighboring points:

$$A(K,L,M) = \frac{1}{2\left[1 + \gamma^2 + \mu^2(1 + \beta^2)\right]} \left\{ \mu^2(1 + \beta^2)[A(K + 1, L, M) + A(K - 1, L, M)] \right.$$

$$+ \gamma^2[A(K, L + 1, M) + A(K, L - 1, M)]$$

$$\left. + A(K, L, M + 1) + A(K, L, M - 1) + \frac{1}{(C - 1)^2} \frac{\partial U}{\partial \xi} \right\} \qquad (44)$$

There is, of course, no need to approximate $\partial U/\partial \xi$ because this differentiation can be analytically found from equation (27) and does not contain the potential function.

The boundary condition $\partial \psi/\partial \xi = 0$, (eq. (30)), which holds at $\xi = 0$ and $\xi = 1$ (the sidewall insulators) must be handled in a way that insures that the approximation does not involve points beyond the region of solution (e.g., points having negative or zero indices). At $\xi = 0$ (K = 1),

$$\frac{\partial \psi}{\partial \xi} \cong \frac{-3A(K, L, M) + 4A(K + 1, L, M) - A(K + 2, L, M)}{2(\Delta \xi)} = 0 \qquad (45)$$

This gives the finite difference form of the boundary condition:

$$A(K, L, M) = \frac{1}{3}[4A(K + 1, L, M) - A(K + 2, L, M)], \quad K = 1 \qquad (46)$$

At $\xi = 1$ (K = C) the approximation is

$$\frac{\partial \psi}{\partial \xi} \cong \frac{A(K - 2, L, M) - 4A(K - 1, L, M) + 3A(K, L, M)}{2(\Delta \xi)} \qquad (47)$$

from which

$$A(K, L, M) = \frac{1}{3}[4A(K - 1, L, M) - A(K - 2, L, M)], \quad K = C \qquad (48)$$

Equation (45) is called a forward difference formula because it involves points forward of the point under consideration. While equation (47) is called a backward difference

formula. There is also a central difference formula:

$$\frac{\partial \psi}{\partial \xi} \cong \frac{A(K+1, L, M) - A(K-1, L, M)}{2(\Delta \xi)} \tag{49}$$

This form obviously does not involve the point A(K, L, M). In considering the boundary conditions at the electrode spacing insulators (eq. (31)) at $\zeta = 0$ and $\zeta = 1$, a forward difference formula for $\partial\psi/\partial\zeta$ must be used at $\zeta = 0$ and a backward difference at $\zeta = 1$. But equation (31) also involves the derivative $\partial\psi/\partial\eta$ for which a central difference formula could be used. However, it was found that the problem would often fail to converge unless a difference formula involving the point A(K, L, M) was used. The reason for this behavior is not clear but may be related to the type of boundary condition given by equation (31), which is neither a Dirichlet nor a Neumann type. Because of this behavior it was decided to use a forward difference at $\zeta = 0$ for both $\partial\psi/\partial\zeta$ and $\partial\psi/\partial\eta$ and a backward difference for both at $\zeta = 1$. Therefore, at $\zeta = 0$ (M = 1), $(1/2) < \eta < 1$, and $[(C + 1)/2 < L < C]$ equation (31) yields

$$A(K, L, M) = \frac{1}{3(1 + \beta\gamma)} \Big\{ \beta\gamma[4A(K, L+1, M) - A(K, L+2, M)] + [4A(K, L, M+1) - A(K, L, M+2)] \Big\} \tag{50}$$

It should be noticed that, at $L = C - 1$, equation (50) contains the point A(K, C + 1, M), which is beyond the range of the mesh points. Points such as these, that overrun the L range, are easily handled by using the periodicity condition.

At $\zeta = 1$ (M = C), $(1/2) < \eta < 1$, and $[(C + 1)/2 < L < C]$

$$A(K, L, M) = \frac{1}{3(1 + \beta\gamma)} \Big\{ \beta\gamma[4A(K, L-1, M) - A(K, L-2, M)] + [4A(K, L, M-1) - A(K, L, M-2)] \Big\} \tag{51}$$

The remaining boundary conditions (eqs. (29) and (32)) are straightforward Dirichlet conditions and will not be rewritten here.

Method of Solution

Because the the large number of points involved in a three-dimensional problem

(for this study $C = 17$ and $C^3 = 4913$ = number of points), a relaxation method must be used to find the $A(K, L, M)$. Direct methods such as a matrix inversion technique would require much more computer storage than is now available. On the other hand, relaxation methods are notorious for oscillatory behavior. This problem can be handled by the dynamic relaxation method in which a damping factor is introduced.

The method used in this report is a modification of the dynamic relaxation method described in reference 8. In that reference an artificial time-dependent problem is added. Equation (1) would then be modified to

$$\operatorname{div} \vec{j} = D \frac{\partial \varphi}{\partial t} + \frac{\partial^2 \varphi}{\partial t^2} \tag{52}$$

where D is a chosen damping factor.

However, for this study, the time dependent portion will be introduced as an auxiliary equation that is solved simultaneously; that is,

$$\operatorname{div} \vec{j} = 0 \tag{53}$$

$$D \frac{\partial \varphi}{\partial t} + \frac{\partial^2 \varphi}{\partial t^2} = 0 \tag{54}$$

In terms of the normalized potential, the derivatives in equation (54) are written:

$$\frac{\partial \psi}{\partial t} \cong \frac{A^{i+1}(K, L, M) - A^{i-1}(K, L, M)}{2(\Delta t)} \tag{55}$$

$$\frac{\partial^2 \psi}{\partial t^2} \cong \frac{A^{i+1}(K, L, M) + A^{i-1}(K, L, M) - 2A^{i}(K, L, M)}{(\Delta t)^2} \tag{56}$$

The superscripts refer to the iteration number. With these substitutions equation (54) is solved for $A^{i+1}(K, L, M)$:

$$A^{i+1}(K, L, M) = \frac{1}{\left(1 + \frac{D\Delta t}{2}\right)} \left[2A^{i}(K, L, M) - A^{i-1}(K, L, M) \left(1 - \frac{D\Delta t}{2}\right) \right] \tag{57}$$

The i^{th} value of $A(K,L,M)$ is the current value as calculated from equation (44) (which is, of course, the reduced form of eq. (53)). Only one complete set of values $A(K,L,M)$ is stored. The set is continually overwritten by the latest calculations. This technique is called Liebman's method (see, e.g., p. 270 of ref. 9) and is the most economical use of computer storage for large iterative problems of the type considered in this report.

At the beginning of each calculation for the potential at (K,L,M) the quantity V is assigned the present value of $A(K,L,M)$, so that

$$V \equiv A^{i-1}(K,L,M) \tag{58}$$

A new value $A^{i}(K,L,M)$ is then calculated from equation (44), and immediately overwritten with $A^{i+1}(K,L,M)$ from equation (57). When the deviation

$$\frac{|A^{i+1}(K,L,M) - V|}{|A^{i+1}(K,L,M)|} \leq \frac{1}{16} \tag{59}$$

for all (K,L,M) the problem is regarded as having converged.

No extensive surveys of the range of the quantity $D\Delta t/2$ has been made. However, it was found that with a $(D\Delta t/2) \cong 0.1$ convergence occurs at about 200 iterations. The problem calculated in reference 8 had 1064 points and requires 92 to 160 iterations depending on boundary conditions.

Preloading a problem with the data from a previous case has a useful effect on the rapidity of convergence. Rarely does a preloaded case require more than 100 iterations and generally about 30 to 50. This is, of course, dependent on the choice of the initial data.

RESULTS

The equipotentials in various planes are plotted for the case of $\mu = \gamma = 1$ (cubic geometry). These results are typical of the structure of the potential function. Two cases are presented: (1) Hall potential equal to 0.25 (approximately midload line) and (2) short circuit (no Hall potential). In both cases a parabolic velocity profile is used $(m = 1)$.

Figure 3 is a plot of the equipotentials in the $\xi = 1/2$ planes for a Hall potential of 0.25. One set of electrodes are located between $L = 1$ and $L = 9$, and a second electrode pair begins at $L = 17$. A region of high electric field is located at the trailing

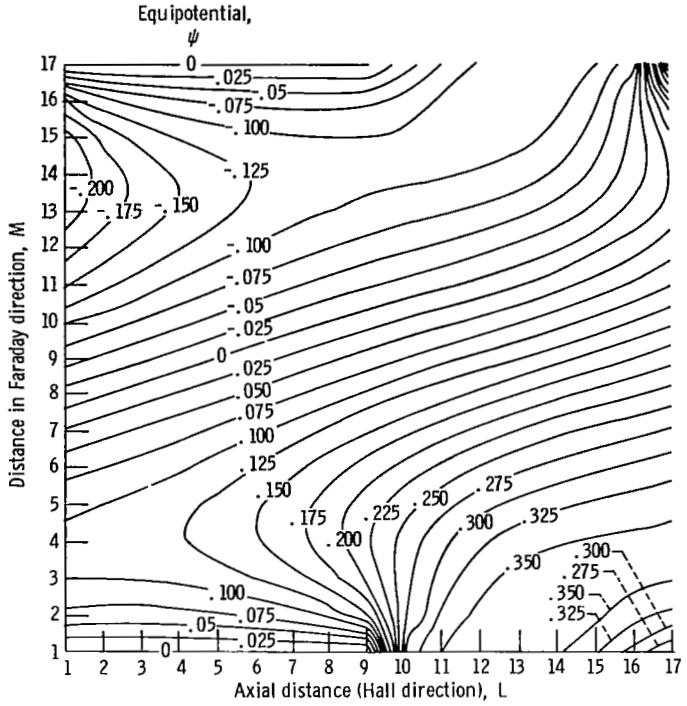

Figure 3. - Equipotentials in (L, M) plane at centerline (K = 9).

edge of the lower electrode, the electron emitter, at $L \simeq 9$. Another point of field concentration is formed at the leading edge of the top Hall electrode, the electron collector, at $L \simeq 16$. These high field regions are characteristic of all the equipotentials that were found. The potential variation along the separating insulator is similar to that found in the two-dimensional studies of references 1 and 2.

The points (5, 9) and (13, 9) have inversion symmetry properties in the (L, M) plane. If an orthogonal cartesian coordinate system is constructed with either point as origin, then a double reflection (first through one axis and a second reflection through the other axis) will leave the potentials unchanged.

Figure 4 shows views of the equipotentials axially down the channel. The velocity is directed into the plane of these figures. Figure 4(a) is the entrance region of the cell (L = 1); part (b) midway across the electrodes (L = 5); part (c) at the trailing edge of the electrodes (L = 9); part (d) midway at the insulators (L = 13); and part (e) at the exit plane of the cell (L = 17). Note that the entrance and exit planes differ only by the Hall potential as is required by the boundary conditions.

Figure 5 is the short-circuit counterpart of figure 3. And figure 6 shows the short-circuit counterparts of figure 4. The slight asymmetry that is shown in the short-circuit plots can be eliminated by tightening the convergence requirement (eq. (57)). This, of course, costs computer time and is only of aesthetic value because the integral

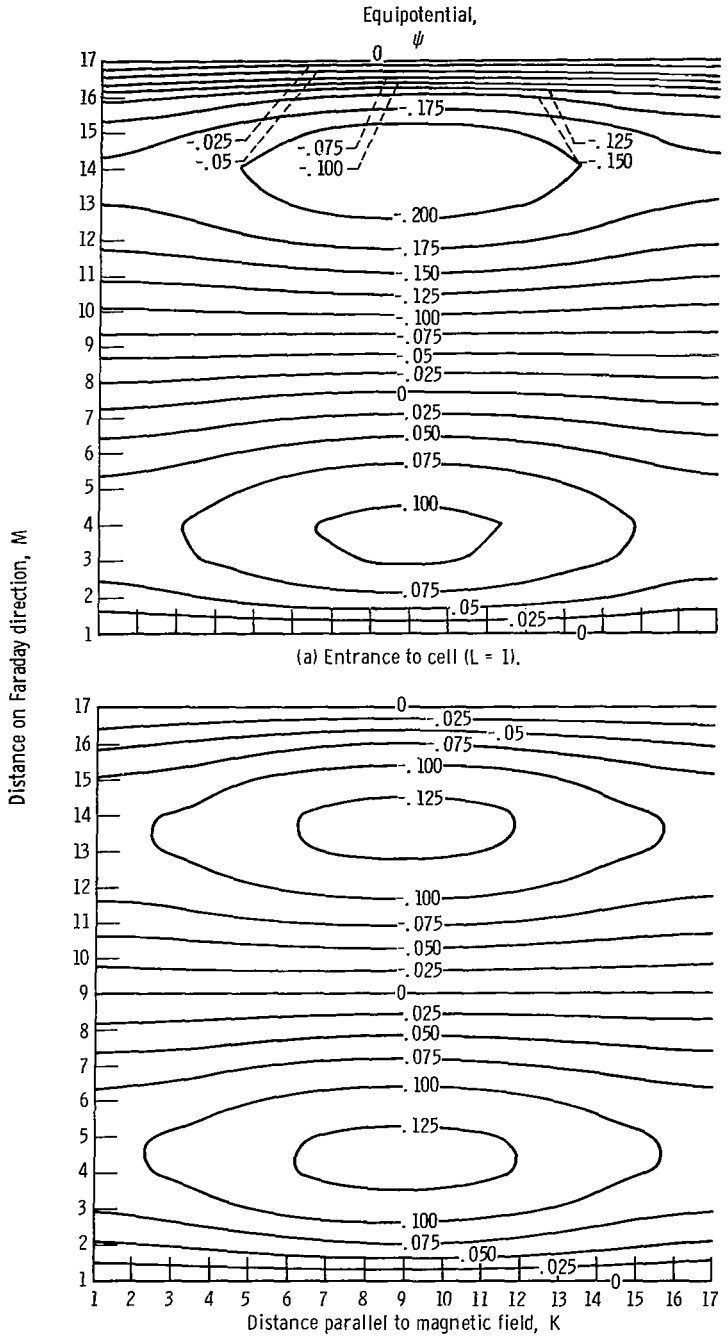

(a) Entrance to cell (L = 1).

(b) Midway across electrode (L = 5).

Figure 4. - Equipotentials in (K, M) plane. Dimensionless Hall potential, 0.25.

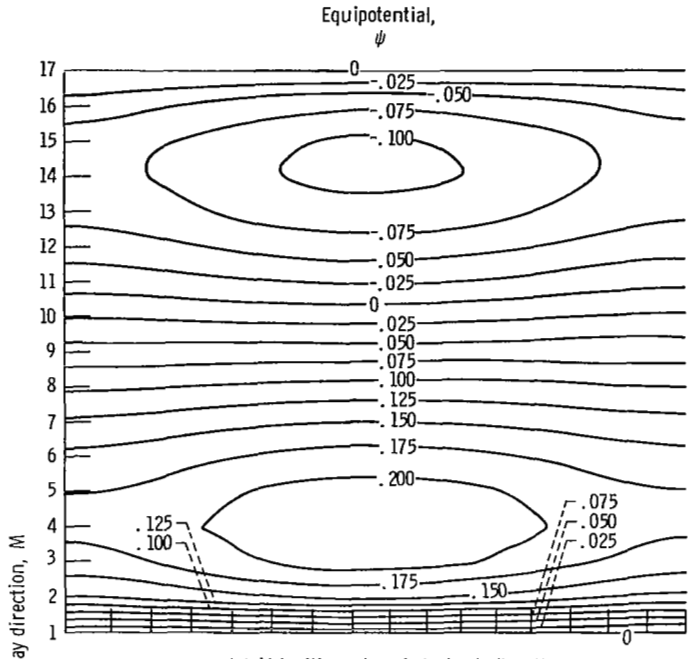

(c) At trailing edge of electrode (L = 9).

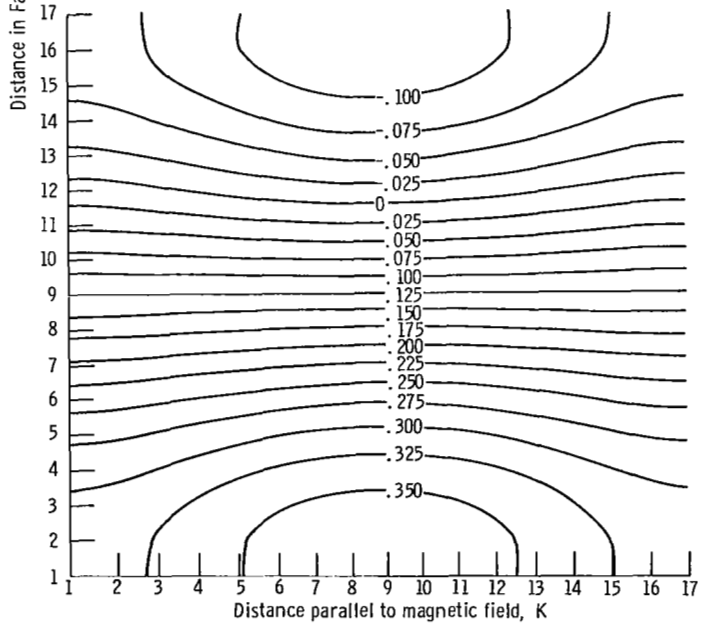

(d) Midway across insulator (L = 13).

Figure 4. - Continued.

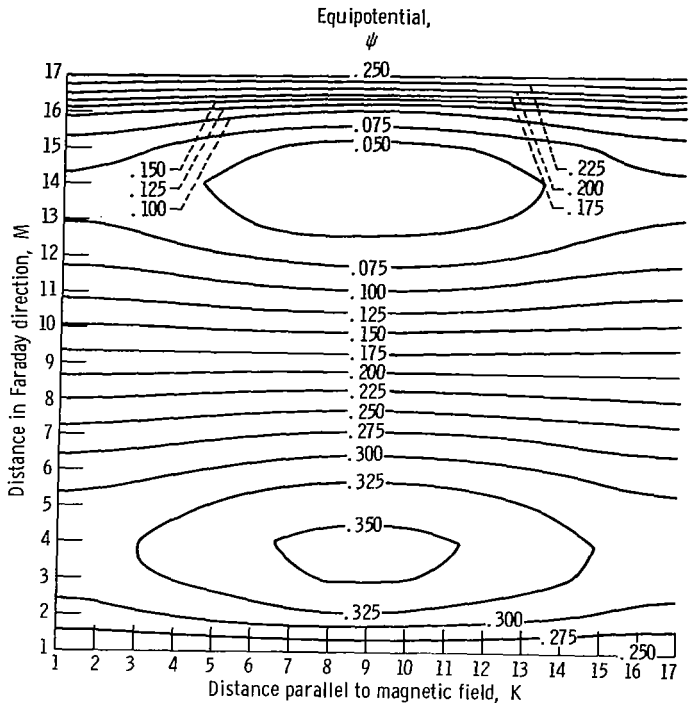

(e) At exit of cell (L = 17).

Figure 4. - Concluded.

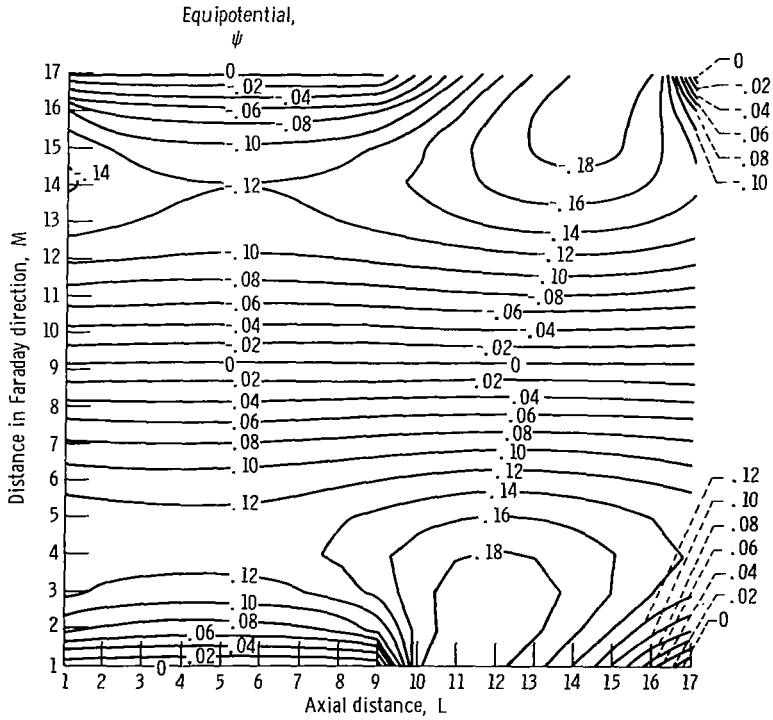

Figure 5. - Short-circuit equipotentials in (L, M) plane (K = 9). Dimensionless Hall potential, 0.

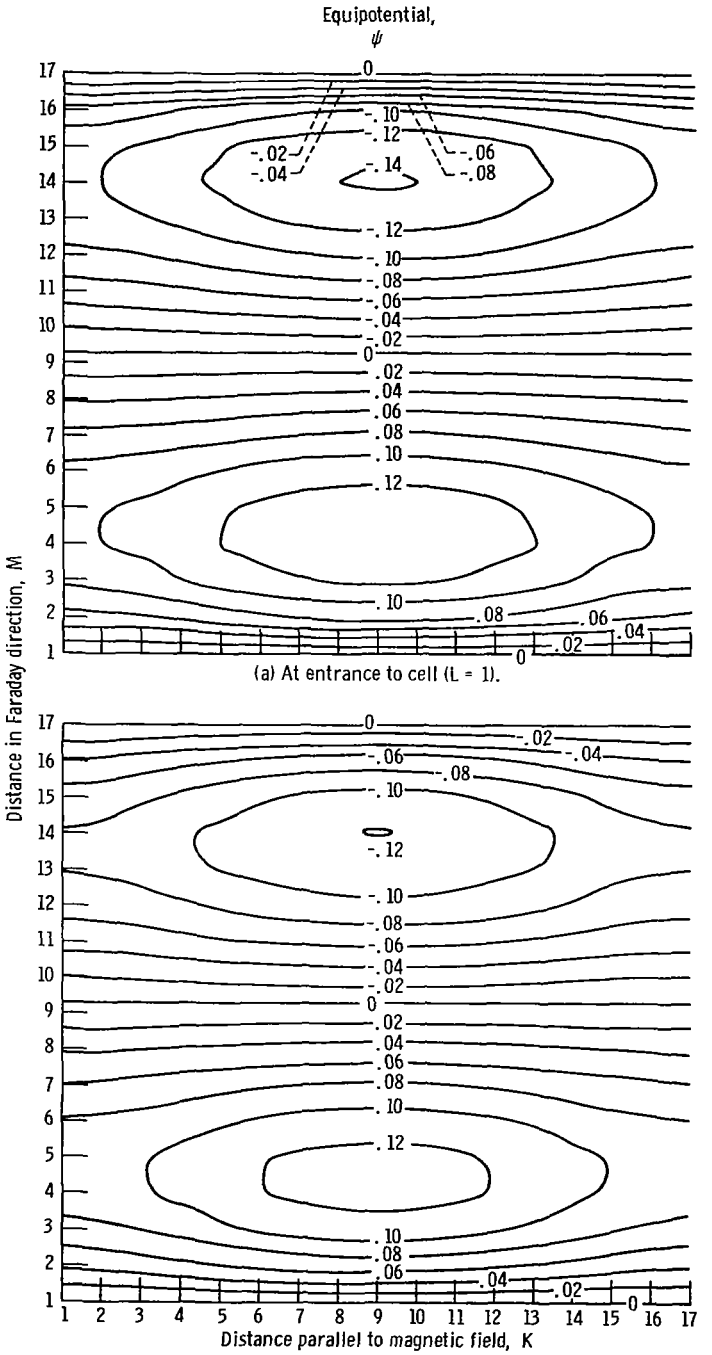

Figure 6. - Short circuit equipotentials in (K, M) plane. Dimensionless Hall potential, 0.

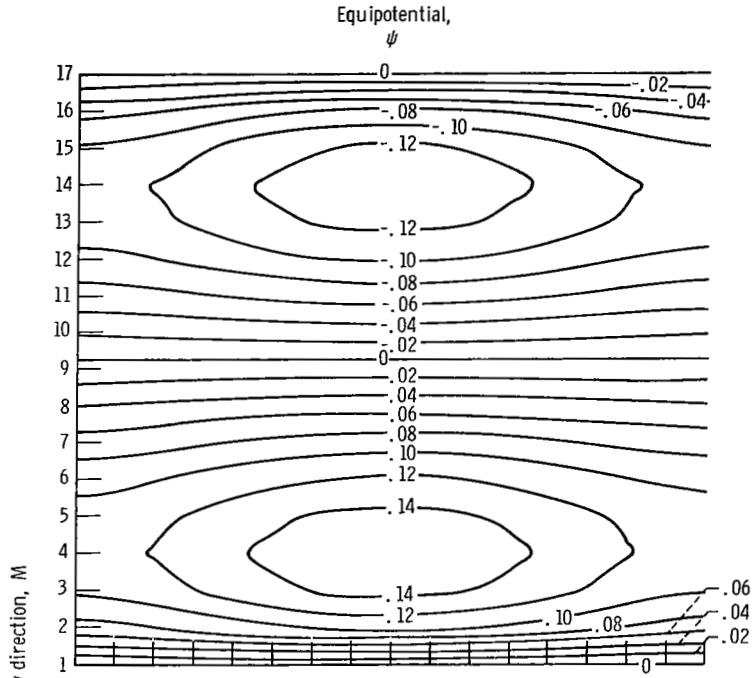

(c) At trailing edge of electrode (L = 9).

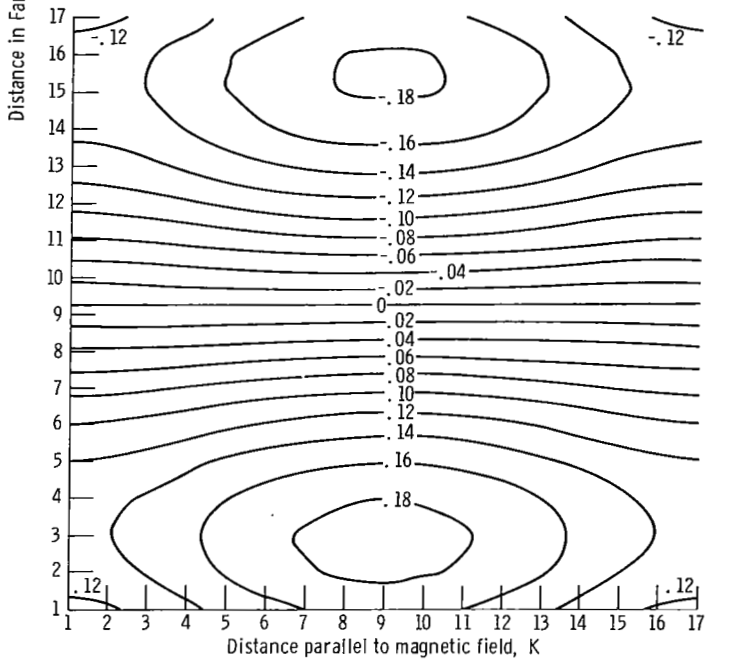

(d) Midway across insulator (L = 13).

Figure 6. - Continued.

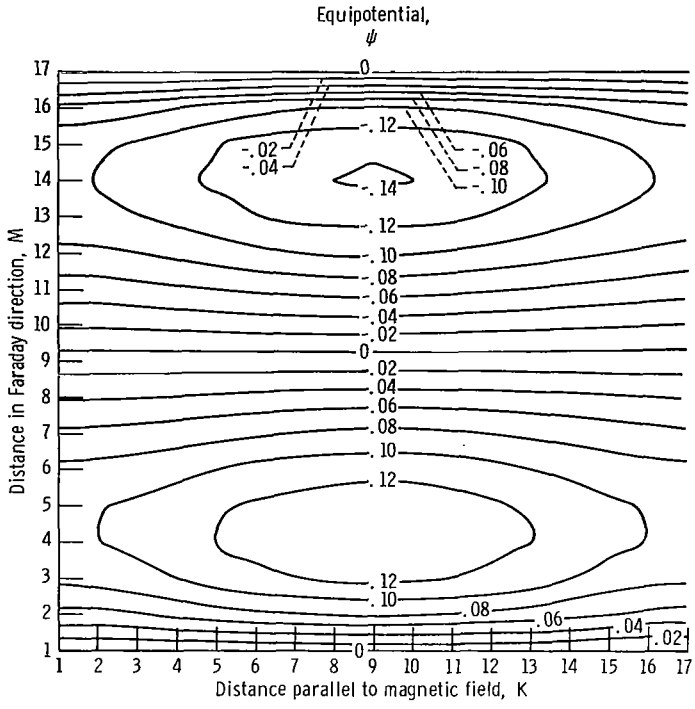

(e) At exit of channel (L = 17).

Figure 6. - Concluded.

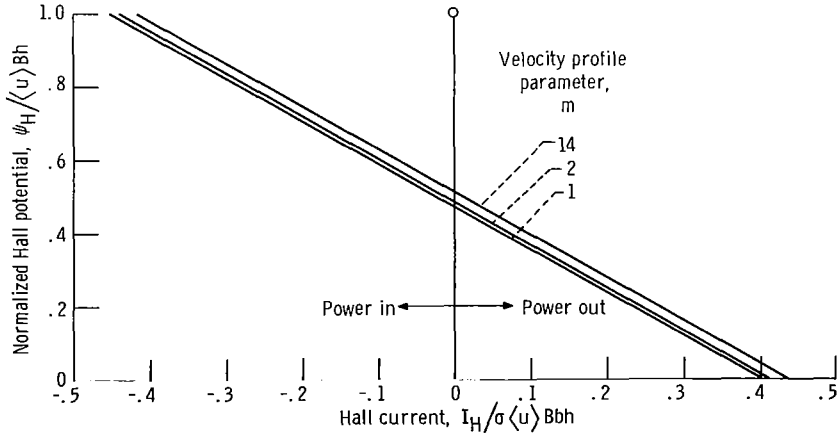

Figure 7. - Hall potential as function of Hall current.

for the Hall current is affected only in the fourth significant figure if the convergence factor in equation (59) is changed to 1/32.

Figures 4 and 6 are graphic displays of the three-dimensionality of the problem. Without a velocity profile, equation (28) could be reduced to a two-dimensional problem by separation of the ξ variable. Because of the boundary condition $\partial\psi/\partial\xi = 0$ at the insulators, the potentials in the (ξ,ζ) or (K,M) plane would be straight lines.

Figure 7 is a plot of Hall potential against Hall current with m (the exponent in the velocity function) as a parameter. Figure 8 is a plot of the Hall current for the cross

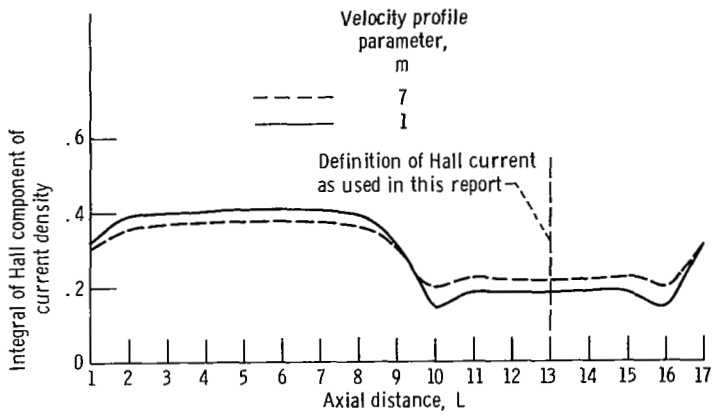

Figure 8. - Integral of Hall component of current density as function of axial distance. Dimensionless Hall potential, 0.25.

sectional planes L = 1 to 17. It illustrates the reason for choosing the plane L = 13 for the definition of the Hall current. Figure 9 is a similar curve of the Hall potential as a function of the absolute value of the Faraday current with m as a parameter. According to reference 5, these load lines can be independent of the velocity profile in the direction parallel to the magnetic field. The effect shown in figures 7 to 9 must be due to the velocity profile in the Faraday direction.

The dependence of figures 7 to 9 on the velocity profile is contrary to the results reported in references 3 and 10. According to these references the load lines are independent of profile. Reference 3, however, posits an arbitrary current dividing line, through which no current can flow in the Hall direction. Reference 10 seems to rest on the assumption that the open-circuit Faraday voltage is defined by letting the Faraday current density vanish identically. This is not realistic because experimentally it is only the total integrated Faraday current that can be set equal to zero.

Figures 7 to 9 can be compared with the two-dimensional analysis of references 1 and 2. For the short-circuit case (zero load factor) the quantity λ defined in reference 2 is equal to the normalized Faraday current plotted in figure 9 of this report. At

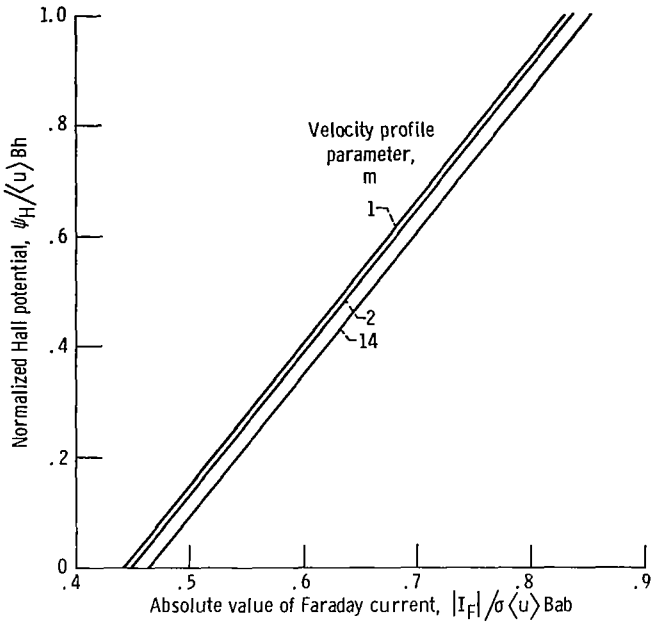

Figure 9. - Hall potential as function of Faraday current.

zero Hall current, figures 7 and 8 show that the Hall potential is 0.47 to 0.51. Figure 9 shows that this is equivalent to a normalized Faraday current of 0.625 to 0.663. The value of λ from reference 2 for the same geometry and Hall parameter is about 0.6. Reference 1 is in agreement with reference 2 for small Hall parameters ($\beta \simeq 1$).

Figure 10 shows the variation of J^2 along the axial distance L at the midpoint of the channel (K = 9). A Hall potential of 0.25 and a turbulent profile (m = 7) was used in the computation. Regions of high J^2 heating are found at the trailing edge of the cathode (lower electrode) and at the leading edge of the anode (upper electrode). Along the centerline of the channel (K = 9, M = 9) the ohmic heating is nearly constant with axial distance L.

A cross plot of figure 10 in the Faraday direction M at L = 5, 9, and 13 is shown in figure 11. The station L = 5 is midelectrode; L = 9 is at the trailing edge of the electrodes; and L = B is midinsulator. The plot shows that J^2 is diminished at the channel walls (electrode-electrode spacing insulator) except for the hot spots near the trailing edge of the cathode.

Figures 12 to 14 show the variation of J^2 at the same stations (L = 5,9,13) between the sidewall insulators. These plots show that the walls are regions of greatly reduced ohmic heating.

Figure 15 shows the variation of J^2 along the channel midplane (K = 9) for a parabolic velocity profile (m = 1). This figure is calculated at the same conditions as figure 10. The only difference being the velocity profile. The same general characteris-

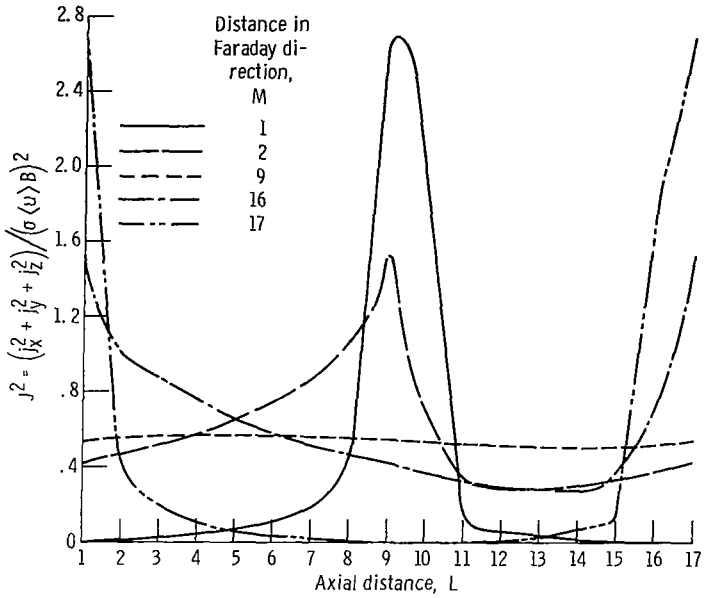

Figure 10. - The square of normalized total current density J^2 distribution as function of axial distance for turbulent profile (m = 7). Midchannel (K = 9); dimensionless Hall potential, 0.25.

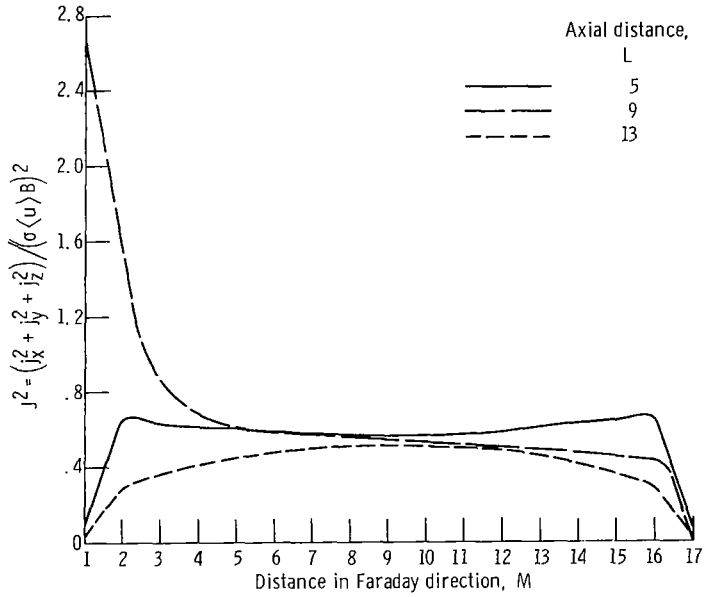

Figure 11. - Distribution of the square of normalized total current density J^2 as function of Faraday distance for turbulent profile (m = 7). Midchannel (K = 9); dimensionless Hall potential, 0.25.

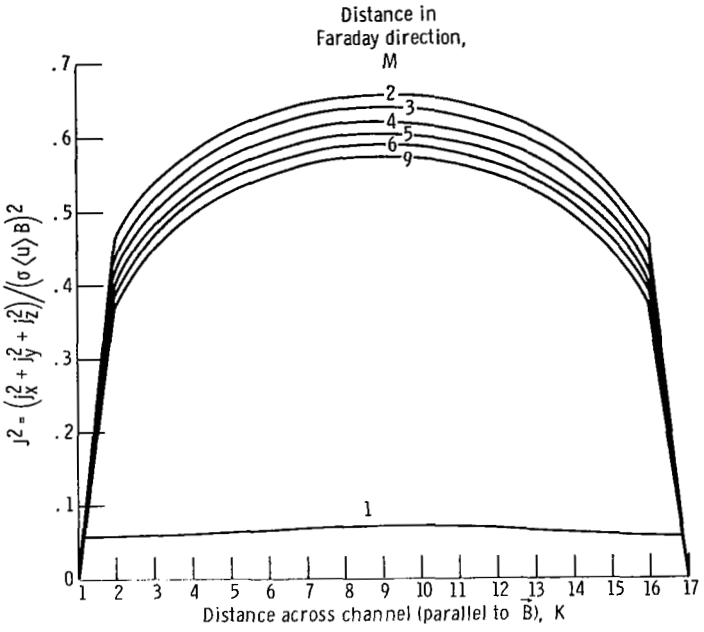

Figure 12. - Distribution of the square of normalized total current density J^2 as function of distance across channel at midelectrode (L = 5) for turbulent profile (m = 7). Dimensionless Hall potential, 0.25.

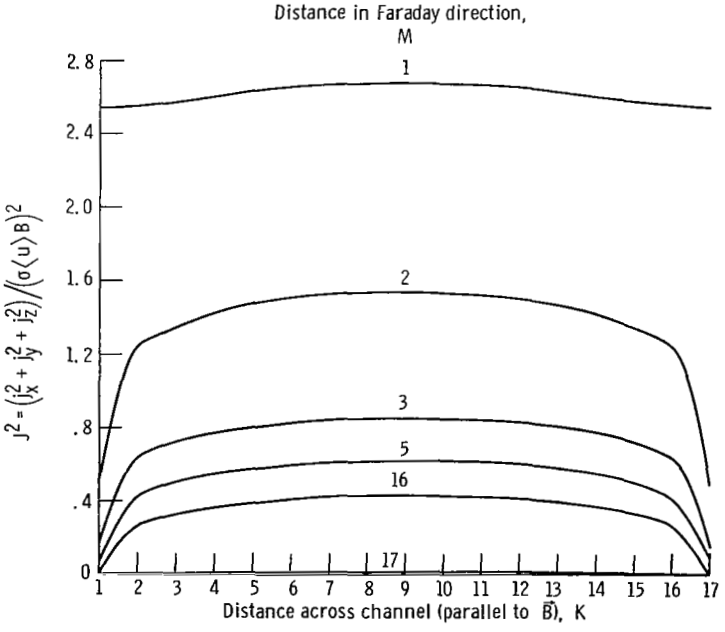

Figure 13. - Distribution of the square of normalized total current density J^2 as function of distance across channel at trailing edge of electrode (L = 9) for turbulent profile (m = 7). Dimensionless Hall potential, 0.25.

TABLE I. - COMPARISON OF INTEGRATED THREE-DIMENSIONAL EFFICIENCY WITH LOCAL EFFICIENCY

Velocity profile parameter, m	Profile	Dimensionless Hall potential, ψ_H	Dimensionless Hall current, J_H	$\psi_H J_H$	Dimensionless ohmic heating,[a] $\frac{1}{\gamma}\int J^2\, d\xi\, d\eta\, d\zeta$	Useful efficiency[b]	Local efficiency[c]	Hall load factor, K_H
1	Parabolic	0.25	0.188	0.047	0.599	0.073	0.163	0.532
7	Turbulent	.25	.219	.054	.457	.106	.168	.492

[a] $\text{Ohmic heating} = \frac{1}{\sigma}\int j^2\, dx\, dy\, dz \equiv abh\sigma(\langle u\rangle B)^2 \int J^2\, d\xi\, d\eta\, d\zeta$.

[b] $\text{Useful efficiency} = \frac{\int \vec{j}\cdot\vec{E}\, dx\, dy\, dz}{\int \vec{j}\cdot\vec{E}\, dx\, dy\, dz + \frac{1}{\sigma}\int j^2\, dx\, dy\, dz} \equiv \frac{\psi_H J_H}{\psi_H J_H + \frac{1}{\gamma}\int J^2\, d\xi\, d\eta\, d\zeta}$.

[c] Ref. 11; eq. 14.17.

The useful power efficiency is 7.3 and 10.6 percent, and this is compared with the local efficiency of 16.3 to 16.8 percent (ref. 11). Thus, volume effects reduce the efficiency by about a factor of two.

The last column in table I gives the integrated ohmic heating for both velocity profiles. The integration is scaled by a factor $abh\sigma(\langle u\rangle B)^2$. Multiplying by this factor will give the ohmic heating per unit volume.

CONCLUSIONS

Electron heating of a plasma moving through a magnetic field is directly proportional to the square of the current density (J^2). Preferential electron heating causes a nonequilibrium conductivity in the plasma.

The phenomenon called boundary-layer shorting presumed that the channel walls were regions of such enhanced conductivity. This view was held because the reduced velocity profile near a wall would result in reduced local electric fields. These local fields drive the current against the induced electrode potentials. Near the walls, however, the local fields are smaller, and it was expected that a large current would flow in the opposite direction and short the adjacent electrodes.

As a result of solving for the three-dimensional potential and current distributions in an MHD generator with various specified velocity profiles and constant conductivity the following conclusions are made:

1. The sidewall insulators of the channel are always regions of lesser J^2 heating than the central portion of the channel (see figs. 12 to 15). Nonequilibrium conductivity is therefore more likely in the central portion than along the sidewalls.

2. The electrode wall insulators (segmentation insulators) are also regions of lesser J^2 heating than in the central portion of the channel, except at the trailing edge of the cathode and at the leading edge of the anode. The gradient of these regions is so steep that, slightly further along the insulator, away from the electrode, the J^2 heating is insignificant (see figs. 10 and 15). Unless these hot spots produce "pockets" of highly conducting plasma that migrate along the insulator to the adjacent electrode, it is difficult to see how shorting can take place.

3. Different velocity profiles provide differently sized regions near the walls in which the local fields are reduced and in which, presumably, the shorting phenomenon might be observed. For all the profiles used in this study, the calculated J^2 distributions are substantially the same in that the walls always have less J^2 heating.

4. Surface effects on the insulator material, such as coating with seed material, are outside the scope of this study. Such effects could explain observed shorting and still be consistant with the results of this study.

Lewis Research Center,
National Aeronautics and Space Administration,
Cleveland, Ohio, September 24, 1971,
112-02.

REFERENCES

1. Hurwitz, H., Jr.; Kilb, R. W.; and Sutton, G. W.: Influence of Tensor Conductivity on Current Distribution in a MHD Generator. J. Appl. Phys., vol. 32, no. 2, Feb. 1961, pp. 205-216.

2. Celinski, Zdzislaw N.; and Fischer, Fred W.: Effects of Electrode Size in MHD Generators with Segmented Electrodes. AIAA J., vol. 4, no. 3, Mar. 1966, pp. 421-428.

3. Schultz-Grunow, F.; and Denzel, D. L.: Evaluation of the Performance Characteristics for a Faraday Generator. Engineering Developments in Energy Conversion. ASME, 1965, pp. 1-14.

4. Lengyel, Lajos L.: Two-Dimensional Current Distributions in Faraday Type MHD Energy Converters Operating in the Nonequilibrium Conduction Mode. Energy Conversion, vol. 9, Mar. 1969, pp. 13-23.

5. Haines, M. G.: An Arbitrary Two-Dimensional Profile of Velocity in a Segmented MHD Duct. Plasma Phys., vol. 10, no. 8, Aug. 1968, pp. 803-805.

6. Deissler, Robert G.; and Taylor, Maynard F.: Analysis of Turbulent Flow and Heat Transfer in Noncircular Passages. NASA TR R-31, 1959.

7. Abramowitz, Milton; and Stegun, Irene A., eds.: Handbook of Mathematical Functions with Formulas, Graphs, and Mathematical Tables. Appl. Math. Ser. 55, National Bureau of Standards, 1964, p. 914.

8. Rushton, K. R.; and Laing, Lucy M.: A Digital Computer Solution of the Laplace Equation Using the Dynamic Relaxation Method. Aeronaut. Quart., vol. 19, Nov. 1968, pp. 375-387.

9. Binns, K. J.; and Lawrenson, P. J.: Analysis and Computation of Electric and Magnetic Field Problems. Macmillan Co., 1963, p. 270.

10. Sutton, George W.; and Sherman, Arthur: Engineering Magnetohydrodynamics. McGraw-Hill Book Co., Inc., 1965, p. 482.

NASA-Langley, 1972 —— 25 E-6551

"The aeronautical and space activities of the United States shall be conducted so as to contribute . . . to the expansion of human knowledge of phenomena in the atmosphere and space. The Administration shall provide for the widest practicable and appropriate dissemination of information concerning its activities and the results thereof."

—NATIONAL AERONAUTICS AND SPACE ACT OF 1958

NASA SCIENTIFIC AND TECHNICAL PUBLICATIONS

TECHNICAL REPORTS: Scientific and technical information considered important, complete, and a lasting contribution to existing knowledge.

TECHNICAL NOTES: Information less broad in scope but nevertheless of importance as a contribution to existing knowledge.

TECHNICAL MEMORANDUMS: Information receiving limited distribution because of preliminary data, security classification, or other reasons.

CONTRACTOR REPORTS: Scientific and technical information generated under a NASA contract or grant and considered an important contribution to existing knowledge.

TECHNICAL TRANSLATIONS: Information published in a foreign language considered to merit NASA distribution in English.

SPECIAL PUBLICATIONS: Information derived from or of value to NASA activities. Publications include conference proceedings, monographs, data compilations, handbooks, sourcebooks, and special bibliographies.

TECHNOLOGY UTILIZATION PUBLICATIONS: Information on technology used by NASA that may be of particular interest in commercial and other non-aerospace applications. Publications include Tech Briefs, Technology Utilization Reports and Technology Surveys.

Details on the availability of these publications may be obtained from:

SCIENTIFIC AND TECHNICAL INFORMATION OFFICE

NATIONAL AERONAUTICS AND SPACE ADMINISTRATION

Washington, D.C. 20546